Real-Time Estimation of Bare-Airframe Frequency Responses from Closed-Loop Data

Jared A. Grauer*
NASA Langley Research Center, Hampton, Virginia, 23681

Matthew J. Boucher†
NASA Armstrong Flight Research Center, Edwards, California, 93523

A method is presented for computing frequency responses of multiple-input multiple-output bare-airframe dynamics from flight test data containing feedback control and/or mixing of control effectors. Orthogonal phase-optimized multisines are used to simultaneously excite each input with unique harmonic frequencies, at which frequency responses are computed as ratios of output-to-input Fourier transform data. The confounding effects of feedback and mixing for frequency response estimation are resolved by interpolating the frequency responses among all the harmonic frequencies. The method can be run in batch for post-flight analysis, or in real time as the aircraft is flying. The effectiveness of the method was verified using closed-loop simulations of the subscale NASA T-2 generic transport airplane. The method was also demonstrated using flight test data from the X-56A MUTT aeroelastic airplane, which was flown with feedback control and mixing.

I. Nomenclature

j = imaginary number, $= \sqrt{-1}$

s = Laplace variable

t = time, s

$|.|$ = magnitude or absolute value

II. Introduction

A common goal in the system identification analysis of aircraft is to determine a bare-airframe dynamics model from measured flight data. However, it is often necessary to fly the aircraft with a control system active, and/or with mixing applied to multiple control effectors. In these cases, inputs become correlated and system identification results degrade [1–3].

*Research Engineer, Dynamic Systems and Control Branch, MS 308, Associate Fellow AIAA.
†Research Engineer, Controls and Dynamics Branch, MS 4840D, Member AIAA.

One solution to this problem is to add different perturbations to each input command, after the control system and mixer. If the perturbations lower the input pairwise correlations below about 0.9 in absolute value, parameter estimation methods such as equation error and output error can be applied in the usual manner to identify bare-airframe dynamics from closed-loop data [1, 2]. This approach was first applied during testing of the open-loop unstable X-29A airplane and has been successfully used in subsequent flight tests with the F-18 HARV, X-31, F-15B ACTIVE, X-43A Hyper-X, T-2 generic transport, X-56A MUTT, and many others.

If frequency responses are used for identification of multiple-input bare-airframe dynamics instead of equation error or output error, additional considerations are necessary when feedback or mixing are present, such as those discussed in Ref. [3] using spectral methods. For moderately correlated inputs, corrections can be applied to condition the data and improve the estimation results. For highly correlated inputs, the indirect approach [4] can be used to retrieve the bare-airframe model from an identified closed-loop model and known control law, or the joint input-output approach can be used to treat the inputs and outputs together as outputs of a separate dynamical system driven by a reference input [4–6]. These additional considerations are irrelevant when the analysis is performed using equation error or output error, with either time series or Fourier transform data [1]. Despite the additional complexity, a non-parametric analysis from frequency responses may be warranted and advantageous in some cases, such as for identifying high-order systems, determining the model structure, and obtaining starting values for model parameters without additional information [3].

A method for frequency response estimation, not using spectral methods, was introduced in Refs. [1, 7]. Orthogonal phase-optimized multisine inputs were used to excite the aircraft dynamics by moving multiple control effectors at the same time but with different harmonic frequencies. Frequency responses were then computed by dividing Fourier transforms of measured output and input data evaluated at the harmonic frequencies in the respective inputs. As noted in Ref. [6], the accuracy of these estimates degrades for multiple-input systems when feedback or mixing is present because an output at a particular harmonic frequency can no longer be uniquely attributed to a single input, which biases the frequency response estimates.

In this paper, the frequency response method in Refs. [1, 7] is extended to account for the effects of feedback and mixing. The estimation problem, involving Fourier transform data of inputs and outputs evaluated at the input harmonic frequencies, was cast as a system of linear equations. When feedback or mixing is present, there are additional evaluations of the frequency responses involved that render the system underdetermined. Interpolation of the frequency responses was developed to provide the supplementary information, and the fully-determined system of linear equations was efficiently solved for the unknown frequency responses using standard numerical routines. In the limit as the amounts of feedback and mixing decrease, the procedure in Refs. [1, 7] is recovered.

The method is useful for estimating frequency responses of multiple-input multiple output (MIMO) systems, with or without feedback and mixing. Because all control effectors can be excited at the same time, rather than sequentially such as with conventional doublet or frequency sweep inputs, flight test durations can be reduced to save time and cost.

Estimated frequency responses can be analyzed post-flight for parametric modeling with transfer function or state-space models [8], or can be computed in real time to check results and data information during a flight test, monitor adaptive control laws, detect sensor and actuator faults, or verify stability margins to expedite envelope expansion testing.

This paper is organized as follows. Section III summarizes the experiment design and the Fourier transform methods. Section IV develops the frequency response method using a series of simulation examples based on the NASA T-2 airplane. Section V demonstrates the method using flight test data for the X-56A airplane, which was flown under closed-loop control and with control surface mixing. All simulation and flight test results showed close agreement with an output-error analysis in the frequency domain, which was not subject to the same issues for identifying bare-airframe models from closed-loop data. Lastly, Section VI discusses conclusions. The MATLAB®-based software package called System IDentification Programs for AirCraft, or SIDPAC [9], was used for the multisine input design, Fourier transforms, and output-error analysis.

III. Experiment Design and Data Analysis

A. Orthogonal Phase-Optimized Multisine Inputs

The orthogonal phase-optimized multisine inputs, subsequently referred to as multisines, were first presented in Refs. [10, 11]. This section summarizes the design of those inputs and discusses advantages and implications for frequency response estimation. For more details on multisines or flight test examples, see Ref. [1] and the references therein.

Multisine inputs are applied over a time duration T, which defines the fundamental frequency $1/T$ of the data record. Harmonic frequencies k/T are included in the multisines, where k is the integer harmonic number. For frequency response estimation, T is a compromise between meeting operational requirements and achieving a fine frequency resolution. The set of n_f included harmonics, K, is selected to span the bandwidth of interest. Good modeling results usually need at least two cycles of each frequency, making $k = 2$ a practical lower limit, although higher values are preferable. If lower frequencies or a finer frequency resolution is desired, T should be increased. When designing multisines for multiple inputs, K is divided into the subsets $K_1, K_2, \ldots, K_{n_u}$, each containing n_{f_j} frequencies. Harmonics are typically assigned to these subsets in an alternating manner so that each input has wide coverage over the excitation bandwidth.

Once the harmonics have been assigned to the inputs, each multisine is constructed as the sum of sinusoids

$$\mu_j(t) = \sum_{k \in K_j} a_k \sin\left(\frac{2\pi k}{T} t + \phi_k\right), \qquad \text{for } j = 1, 2, \ldots, n_u \tag{1}$$

The amplitudes a_k are designed according to desired power spectra for each input. A uniform distribution could be chosen or values of a_k could be tailored for specific applications, such as avoiding known structural resonances or

reducing excessive airspeed variation from phugoid motions. The phase angles ϕ_k are optimized for each input to minimize the ratio of peak-to-peak amplitude to a measure of input energy, called relative peak factor (RPF). This optimization helps to keep the aircraft near the target flight condition, which is important for linear modeling.

Multisine inputs have many characteristics that are advantageous for frequency response estimation. Because they are summations of unique harmonic sinusoids, multisines are mutually orthogonal and therefore can be applied to multiple inputs simultaneously for system identification. Although a control law will raise the level of input correlation, adding orthogonal perturbations to the input commands typically results in inputs with low correlations. Another benefit is that after initial transient responses decay, multisines elicit steady-state responses, which is the information needed to estimate frequency responses. Multisines are analogous to single-sinusoid dwells used in early experiments for frequency response identification [12], but can include many frequencies on many inputs instead of a single frequency on a single input, significantly reducing flight time and cost. In addition, multisines are symmetric and small-amplitude perturbations that keep the aircraft near the target flight condition. Lastly, no more prior information about the system is needed to design a multisine than is needed to design multi-step or frequency sweep inputs.

B. Fourier Transforms

To estimate frequency responses, measured data are first transformed from the time domain to the frequency domain. The analytical tool for this process is the finite Fourier transform

$$x(\omega) = \int_0^T x(t)\, e^{-j\omega t}\, dt \tag{2}$$

where $x(t)$ and $x(\omega)$ are Fourier transform pairs, and where ω is the radian frequency.

Equation (2) can be evaluated in several ways. Fast Fourier transform (FFT) routines are often too coarse in the bandwidth of interest for flight dynamics applications. Rather, a high-accuracy finite Fourier transform based on the chirp z-transform and cubic interpolation of the measured data can be used in post-flight analysis when the entire data record is available [1]. Alternatively, when the sampling rate is much higher than the bandwidth of interest, the Euler approximation

$$x(\omega) \simeq \Delta t \sum_{i=1}^{N} x(t_i)\, e^{-j\omega t_i} \tag{3}$$

can be used to approximate Eq. (2), where Δt is the sampling period and N is the number of samples. This form can be made recursive for real-time analysis during flight as

$$x_i(\omega) = \lambda\, x_{i-1}(\omega) + x(t_i)\, e^{-j\omega t_i} \tag{4}$$

where transforms are updated with each new data sample. The term λ is an exponential forgetting factor that can

Fig. 1 NASA T-2 airplane (credit: NASA Langley Research Center).

be adjusted between 0 and 1 to systematically discard past data and adapt more quickly to recent information. The computational simplicity of Eq. (4) enables the analysis of many measurements and many frequencies with low computational requirements.

IV. Method Development and Simulation Results

This section develops the frequency response estimation method using a series of simulation examples based on the short period dynamics of the NASA T-2 subscale airplane. First, the simulation model and multisine inputs are presented. Second, the model was simulated in the open-loop configuration and frequency responses were estimated using the basic approach introduced in Refs. [1, 7]. Next, pitch rate was fed back to one input, and the inadequacy of the basic approach in this situation is discussed, as well as solution strategies. Pitch rate was then fed back to both inputs and the general approach for frequency response estimation with arbitrary feedback and mixing is formalized. Lastly, real-time estimation is demonstrated using the general approach with both inputs containing feedback.

A. T-2 Short Period Simulation

The NASA T-2 airplane, shown in Fig. 1, is a dynamically-scaled 5.5% version of a generic commercial transport aircraft and has been used extensively for flight test research. Its short period dynamics were selected for investigation because they are relatively simple but exhibit the relevant issues when identifying MIMO bare-airframe dynamics from closed-loop data using frequency responses.

The two inputs of the short period model were the symmetric pairs of outboard and inboard elevator surfaces δ_{eo} and δ_{ei}, and the two outputs were pitch rate, q, and vertical acceleration at the center of mass, a_z. Stability and control derivatives were identified from flight test data with the aircraft undergoing small perturbations about straight and level flight at 4.0 deg angle of attack, 130 ft/s airspeed, 1270 ft altitude, and with 1.59 slug mass. The transfer function matrix

Table 1 Measurement noise levels for the T-2 simulation.

Measurement	Standard deviation	Unit
δ_{eo}, δ_{ei}	0.031	deg
q	0.41	deg/s
a_z	0.010	g

representation of the bare-airframe dynamics was

$$\mathbf{H}(s) = \begin{bmatrix} \frac{q(s)}{\delta_{eo}(s)} & \frac{q(s)}{\delta_{ei}(s)} \\ \frac{a_z(s)}{\delta_{eo}(s)} & \frac{a_z(s)}{\delta_{ei}(s)} \end{bmatrix} = \frac{\begin{bmatrix} -18.1s - 36.0 & -18.1s - 36.0 \\ -0.382s^2 - 0.401s + 146 & -0.382s^2 - 0.401s + 146 \end{bmatrix}}{s^2 + 5.13s + 35.1} \tag{5}$$

The transfer functions involving δ_{eo} were the same for δ_{ei} because the identified control derivatives were statistically identical between the two pairs of surfaces. The short period mode had damping ratio 0.43 and natural frequency 5.9 rad/s (0.94 Hz).

Figure 2 shows a block diagram of a pitch-rate feedback control architecture surrounding the bare airframe, which was simulated at 50 Hz. The inputs u_1 and u_2 were δ_{eo} and δ_{ei}, and the outputs y_1 and y_2 were q and a_z. Each of these four signals was passed through sensor dynamics, S, and was added to Gaussian white noise sequences, v, to model the measurements, which are denoted with the m subscript. The sensor dynamics were negligible but were included to discuss their effects in the next section. Measurement noise levels are listed in Table 1 and were identified from flight test data in calm air. Actuator models were previously identified from flight test data as

$$A_j(s) = \frac{u_j(s)}{u_{j_c}(s)} = \frac{31.4}{s + 31.4} e^{-0.01s} \tag{6}$$

where the actuator commands, u_{j_c}, consist of inputs from the pilot, η, multisine inputs, μ, and pitch-rate feedback signals. The blue and red colors for the multisine inputs are used throughout the simulation examples to distinguish between sets of harmonic frequencies.

The multisines used for all simulation examples are parameterized in Table 2. A duration of $T = 20$ s was chosen to give a relatively fine frequency resolution. The bandwidth of excitation was between 0.2–1.55 Hz, in 0.05 Hz increments, which resulted in 28 harmonic frequencies or 14 frequencies per input. The amplitude spectra had equal power at each frequency and were scaled to realistic values used in flight tests.

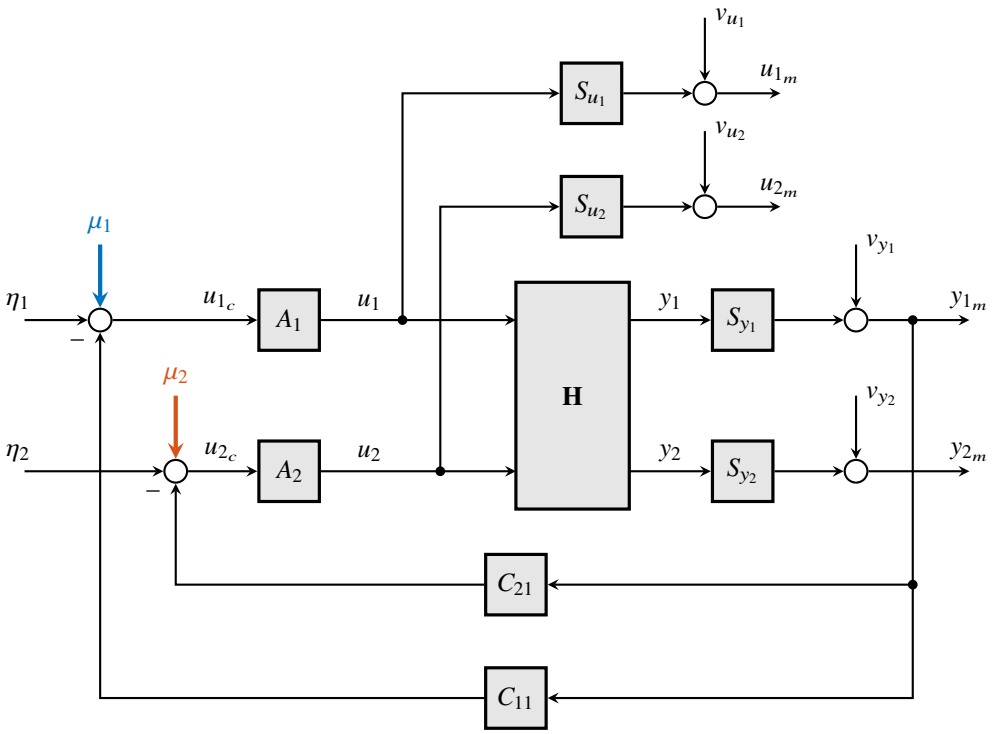

Fig. 2 Block diagram for the T-2 simulation.

Table 2 Multisine design parameters for the T-2 simulation, $T = 20$ s.

Outboard elevator RPF = 1.01				Inboard elevator RPF = 1.06			
a_k, deg	k	k/T, Hz	ϕ_k, rad	a_k, deg	k	k/T, Hz	ϕ_k, rad
0.5345	4	0.20	0.6210	0.5345	5	0.25	4.9405
0.5345	6	0.30	5.1588	0.5345	7	0.35	3.2615
0.5345	8	0.40	1.6756	0.5345	9	0.45	2.0905
0.5345	10	0.50	6.2174	0.5345	11	0.55	2.9055
0.5345	12	0.60	2.6949	0.5345	13	0.65	2.5789
0.5345	14	0.70	3.4949	0.5345	15	0.75	0.2588
0.5345	16	0.80	3.5085	0.5345	17	0.85	4.5254
0.5345	18	0.90	4.2438	0.5345	19	0.95	2.7021
0.5345	20	1.00	3.2842	0.5345	21	1.05	3.2274
0.5345	22	1.10	1.9731	0.5345	23	1.15	4.1436
0.5345	24	1.20	1.5450	0.5345	25	1.25	5.5348
0.5345	26	1.30	4.2009	0.5345	27	1.35	2.7004
0.5345	28	1.40	5.3651	0.5345	29	1.45	6.2552
0.5345	30	1.50	2.6818	0.5345	31	1.55	1.3213

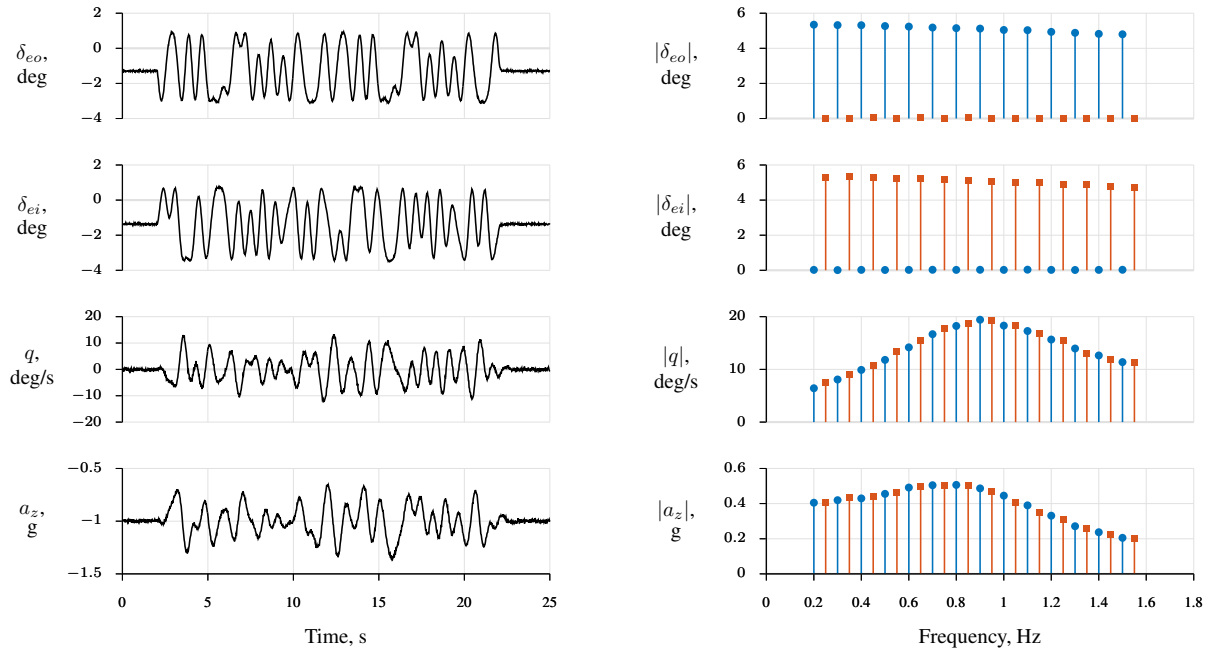

(a) Time histories.

(b) Fourier transform magnitudes.

Fig. 3 T-2 simulation data in the open-loop configuration.

B. Open Loop

The simulation model was first run in the open-loop configuration without feedback control, i.e. $C_{11} = C_{21} = 0$, and measurements are shown in Fig. 3(a). The multisines, shown in the first two plots, had a pairwise correlation of 0. The signal-to-noise ratios for all signals were high at above 17, and the response perturbation magnitudes were similar to those in flight test data.

Fourier transform magnitudes of the measurements are shown in Fig. 3(b). The transforms were only evaluated at the 28 harmonic frequencies because only those frequencies contained power in the inputs and steady-state responses. For these plots, blue circles indicate harmonic frequencies used for δ_{eo}, and red squares indicate harmonic frequencies used for δ_{ei}. Note the control surface deflections each contained power for a single set of unique harmonic frequencies — this will not be the case in later examples with feedback. The responses, however, contained power at all 28 harmonic frequencies because of the MIMO coupling of the dynamics.

To compute frequency response estimates of the bare-airframe dynamics from this data, each of the n_y outputs can

be expanded using transfer function algebra as

$$\begin{aligned} y_{i_m} &= S_{y_i} y_i + v_{y_i} \\ &= S_{y_i} \left[H_{i1} u_1 + H_{i2} u_2 \right] + v_{y_i} \\ &= S_{y_i} \left[H_{i1} \, S_{u_1}^{-1} \left(u_{1_m} - v_{u_1} \right) + H_{i2} \, S_{u_2}^{-1} \left(u_{2_m} - v_{u_2} \right) \right] + v_{y_i} \end{aligned} \tag{7}$$

to show contributions of the sensor dynamics, measurements, and bare-airframe frequency responses. Measurement noise or error in the sensor models can degrade the accuracy of frequency response estimates. However, sensors can typically be characterized well and are usually selected to have negligible dynamics in the bandwidth of interest. Furthermore, good multisine designs achieve high signal-to-noise ratios. Although measurement noise and sensor dynamics may be considered in the analysis, these effects can often be neglected (which was done in the remaining development) so that $y_{i_m} \simeq y_i$, $u_{j_m} \simeq u_j$, and $S_{y_i} = S_{u_j} = 1$, simplifying Eq. (7) to

$$y_i = H_{i1} \, u_1 + H_{i2} \, u_2 \tag{8}$$

Evaluating Eq. (8) at each harmonic frequency results in a system of linear equations of the form $\mathbf{b} = \mathbf{A}\mathbf{x}$, which is a fundamental problem of linear algebra. For the open-loop case, $\mathbf{A}$ has dimensions $(n_y \cdot n_f) \times (n_y \cdot n_u \cdot n_f)$ and is not a square matrix. The system can be partitioned as

$$\begin{bmatrix} \mathbf{b}_1 \\ \\ \mathbf{b}_2 \end{bmatrix} = \begin{bmatrix} \mathbf{A}_{11} & \mathbf{0} \\ \\ \mathbf{0} & \mathbf{A}_{22} \end{bmatrix} \begin{bmatrix} \mathbf{x}_1 \\ \\ \mathbf{x}_2 \end{bmatrix} \tag{9}$$

Letting vectors $\boldsymbol{\omega}_1$ and $\boldsymbol{\omega}_2$ represent the respective frequencies in K_1 and K_2, the $(n_y \cdot n_{f_i}) \times 1$ partitions

$$\mathbf{b}_1 = \begin{bmatrix} y_1(\boldsymbol{\omega}_1) \\ \\ y_2(\boldsymbol{\omega}_1) \end{bmatrix}, \qquad \mathbf{b}_2 = \begin{bmatrix} y_1(\boldsymbol{\omega}_2) \\ \\ y_2(\boldsymbol{\omega}_2) \end{bmatrix} \tag{10}$$

are the measured outputs, evaluated at the two sets of harmonic frequencies. Similarly, the $(n_y \cdot n_u \cdot n_{f_i}) \times 1$ partitions

$$\mathbf{x}_1 = \begin{bmatrix} H_{11}(\boldsymbol{\omega}_1) \\ \\ H_{21}(\boldsymbol{\omega}_1) \\ \\ H_{12}(\boldsymbol{\omega}_1) \\ \\ H_{22}(\boldsymbol{\omega}_1) \end{bmatrix}, \qquad \mathbf{x}_2 = \begin{bmatrix} H_{11}(\boldsymbol{\omega}_2) \\ \\ H_{21}(\boldsymbol{\omega}_2) \\ \\ H_{12}(\boldsymbol{\omega}_2) \\ \\ H_{22}(\boldsymbol{\omega}_2) \end{bmatrix} \tag{11}$$

are evaluations of the bare-airframe frequency responses at ω_1 and ω_2. Lastly, the $(n_y \cdot n_{f_i}) \times (n_y \cdot n_u \cdot n_{f_i})$ partitions

$$\mathbf{A}_{11} = \begin{bmatrix} d\{u_1(\omega_1)\} & \mathbf{0} & d\{u_2(\omega_1)\} & \mathbf{0} \\ \mathbf{0} & d\{u_1(\omega_1)\} & \mathbf{0} & d\{u_2(\omega_1)\} \end{bmatrix} \tag{12a}$$

$$\mathbf{A}_{22} = \begin{bmatrix} d\{u_1(\omega_2)\} & \mathbf{0} & d\{u_2(\omega_2)\} & \mathbf{0} \\ \mathbf{0} & d\{u_1(\omega_2)\} & \mathbf{0} & d\{u_2(\omega_2)\} \end{bmatrix} \tag{12b}$$

are assembled from the measured inputs, where $d\{.\}$ constructs a diagonal matrix from the argument.

The frequency responses at the harmonic frequencies are computed by solving the system for $\mathbf{x}$. Normally, Eq. (9) is underdetermined because there are n_u times as many unknowns as there are equations. However, in the open-loop case with no pilot input,

$$u_1(\omega_2) = A_1(\omega_2)\,\mu_1(\omega_2) = \mathbf{0} \tag{13a}$$

$$u_2(\omega_1) = A_2(\omega_1)\,\mu_2(\omega_1) = \mathbf{0} \tag{13b}$$

by definition and as seen in Figs. 2 and 3(b). Applying this substitution nulls half the elements along diagonals of $\mathbf{A}_{11}$ and $\mathbf{A}_{22}$, reducing the system to

$$\begin{bmatrix} y_1(\omega_1) \\ y_2(\omega_1) \\ y_1(\omega_2) \\ y_2(\omega_2) \end{bmatrix} = \begin{bmatrix} d\{u_1(\omega_1)\} & \mathbf{0} & \mathbf{0} & \mathbf{0} \\ \mathbf{0} & d\{u_1(\omega_1)\} & \mathbf{0} & \mathbf{0} \\ \mathbf{0} & \mathbf{0} & d\{u_2(\omega_2)\} & \mathbf{0} \\ \mathbf{0} & \mathbf{0} & \mathbf{0} & d\{u_2(\omega_2)\} \end{bmatrix} \begin{bmatrix} H_{11}(\omega_1) \\ H_{21}(\omega_1) \\ H_{12}(\omega_2) \\ H_{22}(\omega_2) \end{bmatrix} \tag{14}$$

in which the reduced $\mathbf{A}$ has the square dimensions $(n_y \times n_f) \times (n_y \times n_f)$. The decoupled, fully-determined system has the solution $\mathbf{x} = \mathbf{A}^{-1}\mathbf{b}$, or

$$\begin{bmatrix} H_{11}(\omega_1) \\ H_{21}(\omega_1) \\ H_{12}(\omega_2) \\ H_{22}(\omega_2) \end{bmatrix} = \begin{bmatrix} d\{\frac{1}{u_1(\omega_1)}\} & \mathbf{0} & \mathbf{0} & \mathbf{0} \\ \mathbf{0} & d\{\frac{1}{u_1(\omega_1)}\} & \mathbf{0} & \mathbf{0} \\ \mathbf{0} & \mathbf{0} & d\{\frac{1}{u_2(\omega_2)}\} & \mathbf{0} \\ \mathbf{0} & \mathbf{0} & \mathbf{0} & d\{\frac{1}{u_2(\omega_2)}\} \end{bmatrix} \begin{bmatrix} y_1(\omega_1) \\ y_2(\omega_1) \\ y_1(\omega_2) \\ y_2(\omega_2) \end{bmatrix} \tag{15}$$

More generally, this solution is also expressed as

$$H_{ij}(\omega_j) = \frac{y_i(\omega_j)}{u_j(\omega_j)} \tag{16}$$

which is the ratio of output and input Fourier transforms at the frequencies contained in the input. This *basic approach* for frequency response estimation was developed in Refs. [1, 7]. Equation (16) is applied for each harmonic in each input and the frequency response matrix is computed at the corresponding frequencies. This method can be used when the test data is representative of a linear system operating in steady state and when each harmonic frequency is applied to a single input.

Computing frequency responses in this manner has several advantages. The analysis is straightforward and does not require tuning or using engineering judgement to select parameters in the calculations. It is applicable to MIMO systems and is simple enough to run in real time during flight with low computational resources. For good signal-to-noise ratios and sufficient time durations, these estimates of the frequency response are accurate and unbiased [4, 13].

Figure 4 shows frequency response estimates for the data from Fig. 3. The plots in the left column, shown as blue circles, had δ_{eo} as input and were computed at harmonics in K_1. Likewise, the plots in the right column, shown as red squares, correspond to δ_{ei} and were computed at the harmonics in K_2. These estimates were practically equal to the true frequency responses of the bare-airframe simulation model, which were computed from Eq. (5) with $s = j\omega$ and shown as solid black lines. Errors from measurement noise and transient responses were small.

Overlaying the true frequency responses in Fig. 4 are dashed purple lines, which are the results of an output-error analysis [1, 14] to estimate stability and control derivatives in a state-space representation of Eq. (5) that best match the model output Fourier transforms to measured frequency-domain output data in a maximum likelihood sense. This analysis was included in these simulation examples to establish a baseline for comparison later in Section V, where actual flight test data was analyzed. When applying output error in this way, it is important that the input correlations remain less than about 0.9 in absolute value, which was the case here. Otherwise, the output-error estimation of bare-airframe models from closed-loop data proceeds normally.

C. Single Loop Closure

In this second simulation example, q was fed back to δ_{ei} with $C_{11} = 0$ and $C_{21} = -0.2$. The closed-loop short period mode had damping ratio 0.70 and frequency 8.0 rad/s (1.3 Hz).

Simulated time histories and Fourier transforms of measurements for this case are shown in Fig. 5(a). Data for δ_{eo} were the same as in the previous example, whereas δ_{ei} contained additional contributions from the feedback. The feedback increased the input pairwise correlation from 0.0 to 0.4, reduced the response amplitudes, and resulted in harmonic frequency content from both K_1 and K_2 on δ_{ei}.

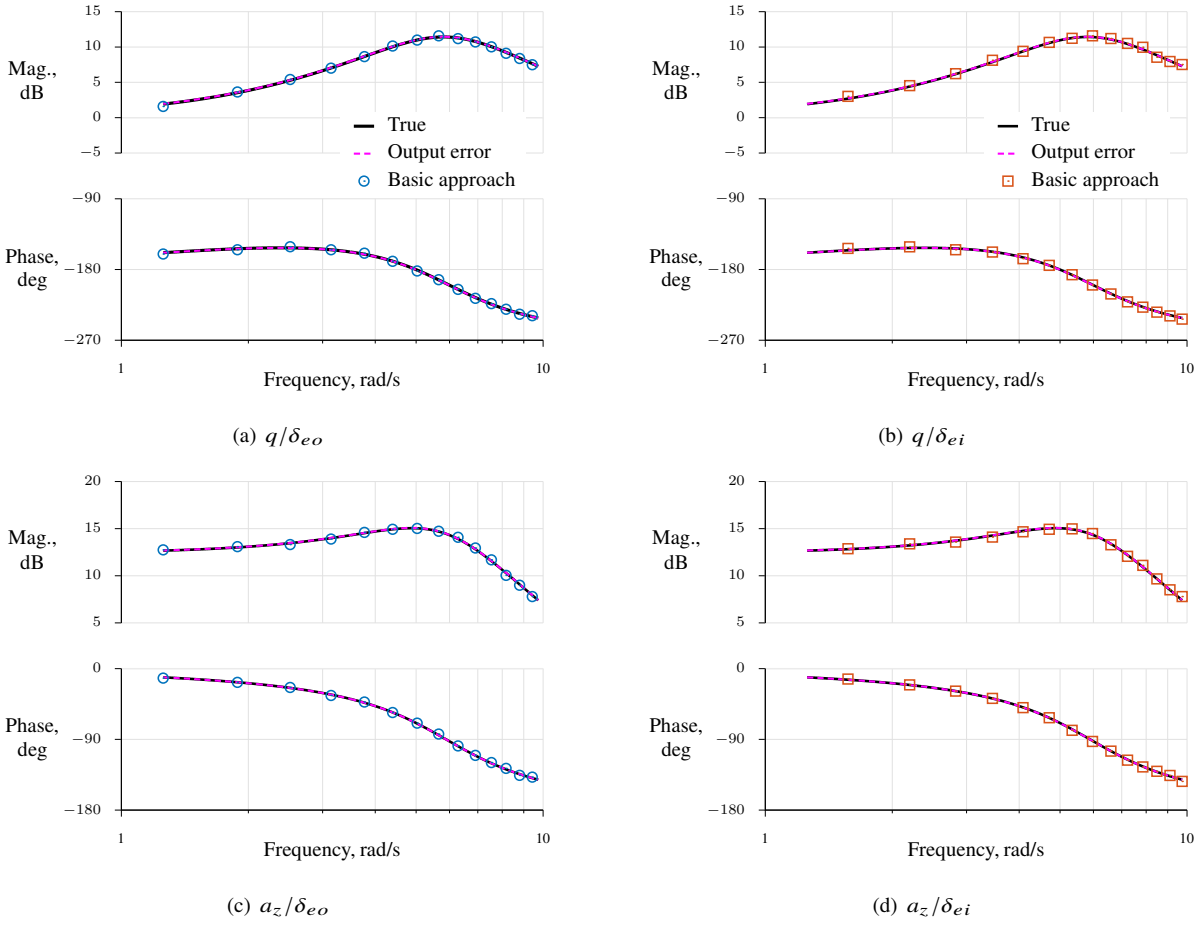

(a) q/δ_{eo} (b) q/δ_{ei}

(c) a_z/δ_{eo} (d) a_z/δ_{ei}

Fig. 4 Frequency response estimates for the T-2 simulation in open-loop configuration.

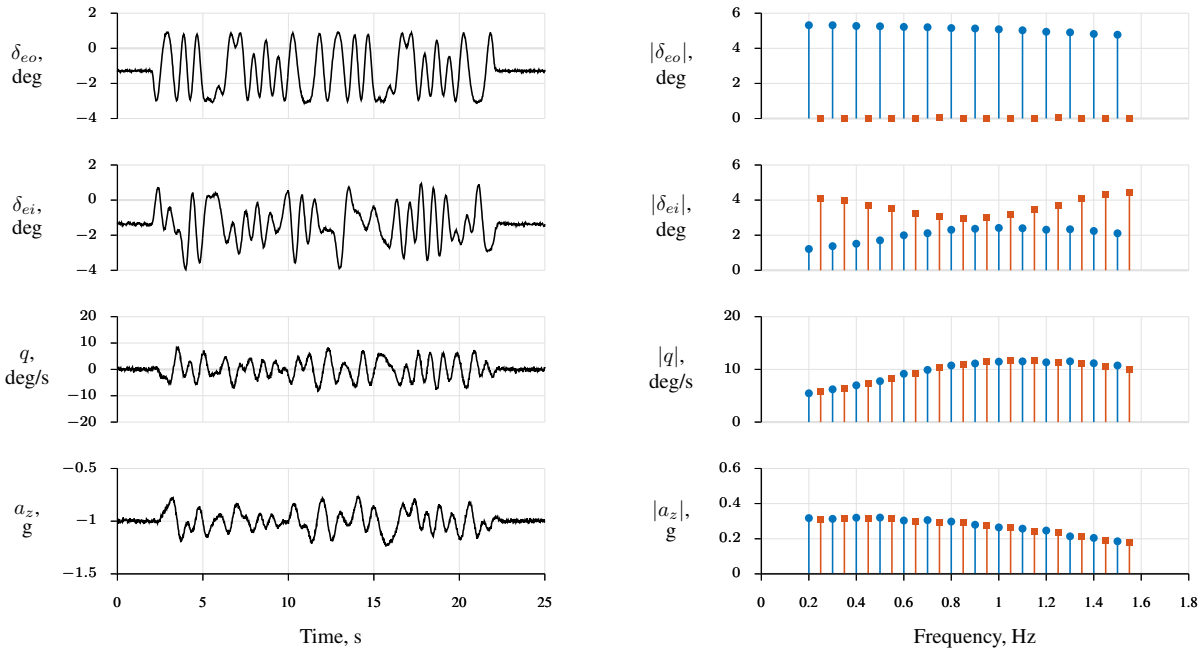

(a) Time histories.

(b) Fourier transform magnitudes.

Fig. 5 T-2 simulation data with single loop closure.

To compute frequency responses from this data, the output responses can again be written as in Eq. (8). From the block diagram for this example, $u_1(\omega_2) = 0$ as before, whereas

$$\begin{aligned} u_2(\omega_1) &= A_2(\omega_1)\left[\mu_2(\omega_1) - C_{21}(\omega_1)\, y_1(\omega_1)\right] \\ &= -A_2(\omega_1)\, C_{21}(\omega_1)\, y_1(\omega_1) \end{aligned} \tag{17}$$

which is nonzero because the steady-state outputs contained power at both sets of harmonic frequencies. In this case, the frequency responses from u_2 (containing feedback) were ratios of Fourier transforms, as in Eq. (16) for the open-loop configuration. However, the frequency responses from u_1 (not containing feedback) were

$$H_{i1}(\omega_1) = \frac{y_i(\omega_1)}{u_1(\omega_1)} - \frac{H_{i2}(\omega_1)\, u_2(\omega_1)}{u_1(\omega_1)} \tag{18}$$

and had additional contributions over the open-loop case. Therefore, $H_{i2}(\omega_2)$ can be calculated using the basic approach, but $H_{i1}(\omega_1)$ needs more information. Note that it is the frequency response with the input *not* containing feedback that is in error when estimated using the basic approach. Also note that as $C_{21} \to 0$, $u_2(\omega_1) \to 0$ and the basic approach is recovered.

There are several strategies for obtaining $H_{i2}(\omega_1)$ from $H_{i2}(\omega_2)$ to compute $H_{i1}(\omega_1)$. Multiple maneuvers using

single-input excitations at the same target flight condition could be combined. Alternatively, the data for $H_{i2}(\omega_2)$ could be fit with a parametric model, such as a transfer function, and then evaluated at the frequencies ω_1. As another option, $H_{i2}(\omega_2)$ could be linearly interpolated for the frequencies ω_1 by recasting the system of linear equations as

$$\begin{bmatrix} \mathbf{b}_1 \\ \mathbf{b}_2 \\ \mathbf{0} \end{bmatrix} = \begin{bmatrix} \mathbf{A}_{11} & \mathbf{0} \\ \mathbf{0} & \mathbf{A}_{22} \\ \mathbf{A}_{31} & \mathbf{A}_{32} \end{bmatrix} \begin{bmatrix} \mathbf{x}_1 \\ \mathbf{x}_2 \end{bmatrix} \tag{19}$$

where the third partitioned row interpolates H_{i2} at frequencies ω_1. Specifically for this example, half the elements in $\mathbf{A}_{22}$ are nulled, $\mathbf{A}_{31}$ has values of $1/2$ along the diagonal and either the super-diagonal or sub-diagonal (depending on the ordering of frequencies), and $\mathbf{A}_{32}$ has values of -1 along the diagonal. The interpolation equations in this *general approach* add enough information to make the reduced system fully determined so that a solution can be computed. For cases of lightly damped modes and coarse frequency resolution, approximation errors from linear interpolation can be reduced by redesigning the multisine inputs for a longer T or using higher-order interpolation.

Frequency response estimates using the simulation data are shown in Fig. 6 using linear interpolation. Estimates computed using the general approach, shown as solid markers, agreed with the true bare-airframe frequency responses. Estimates using the basic approach, shown as open markers, were correct for δ_{ei} but exhibited significant magnitude and phase errors for δ_{eo}, as expected. Cubic interpolation was also investigated, but the estimates had negligible increases in accuracy. Results from an output-error analysis matched the true frequency responses because the control surface correlations were low. Figure 6 shows that the results from the general method with feedback control are of the same excellent quality seen earlier using the basic approach in the open-loop case.

Frequency responses computed from closed-loop data using the basic approach would be correct for $H_{i2}(\omega_2)$ but incorrect for $H_{i1}(\omega_1)$. This was demonstrated in Ref. [6] and is the result of neglecting the second term on the right side of Eq. (18). When considering multiple inputs with feedback or mixing, the bare-airframe dynamics can be accurately computed from closed-loop data using the general approach.

In general, as feedback gains increase, the open-loop and closed-loop frequency responses become more different and the errors incurred from not accounting for feedback or mixing on multiple inputs become larger. However, as shown in this example, even small amounts of feedback can lead to significant errors in the frequency response estimates of the bare-airframe dynamics. This characteristic is sensitive to fewer inputs because each input impacts a larger fraction of the total response.

When conducting flight tests with multisines, pilots are directed not to supply additional inputs, so that $\eta = 0$. The multisines are balanced about zero and keep the aircraft near the target flight condition. If additional inputs are deemed necessary, pilots are asked to make them "low and slow" to keep the added frequency content low in amplitude and

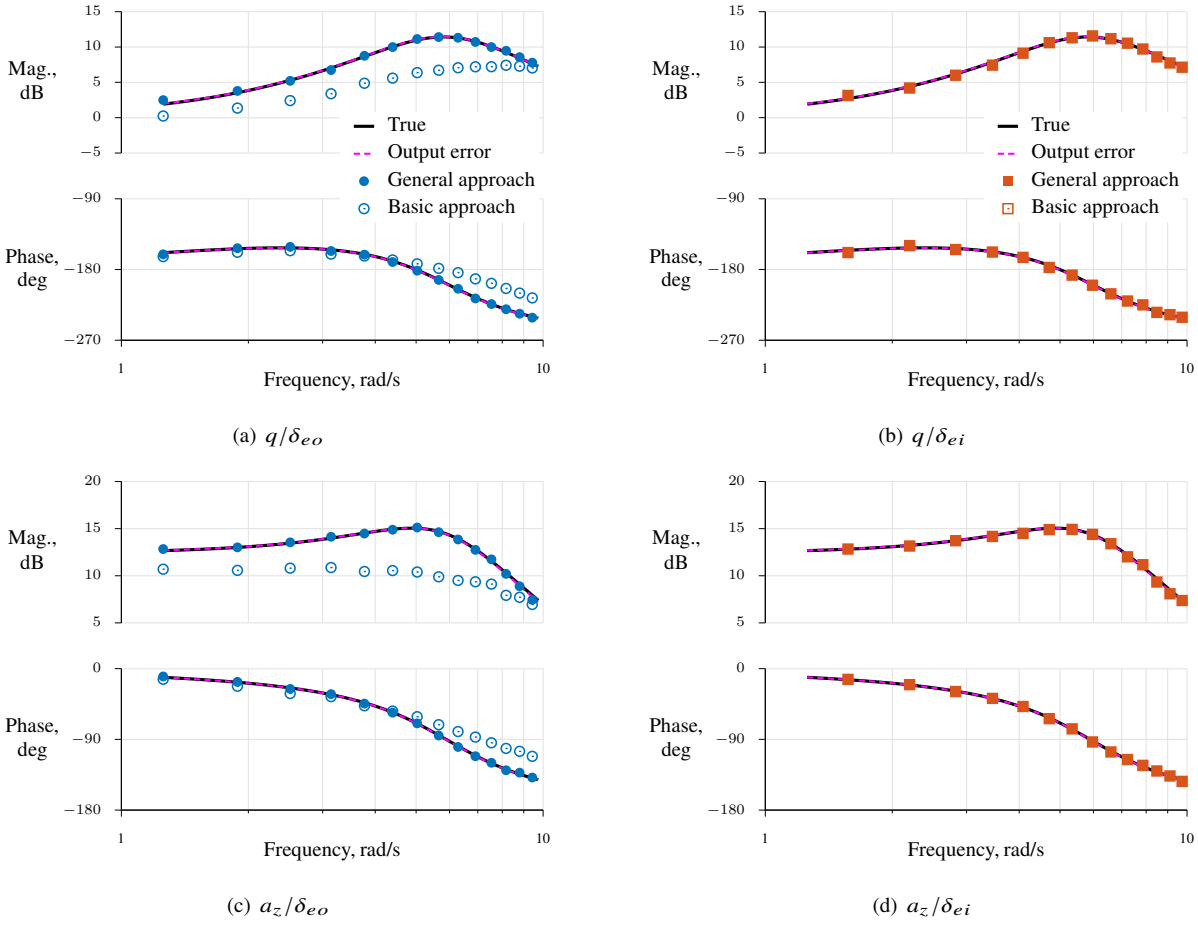

(a) q/δ_{eo} (b) q/δ_{ei}

(c) a_z/δ_{eo} (d) a_z/δ_{ei}

Fig. 6 Frequency response estimates for T-2 simulation with single loop closure.

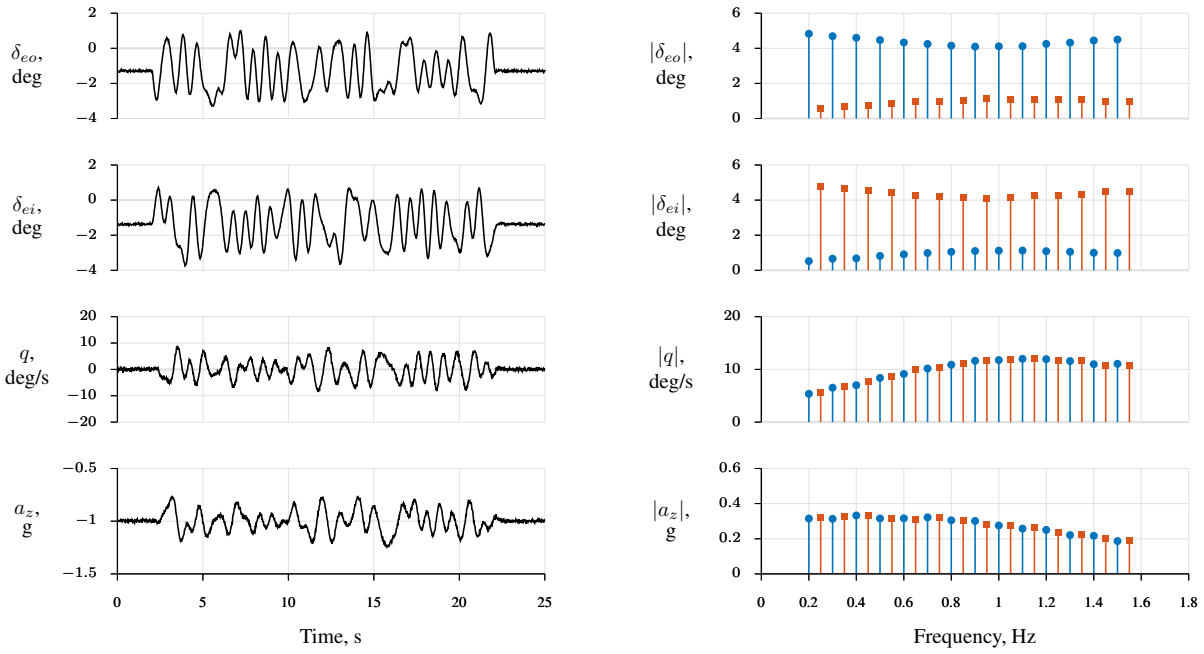

(a) Time histories.

(b) Fourier transform magnitudes.

Fig. 7 T-2 simulation data with multiple loop closures.

below the bandwidth of the multisines.

In the limit for high feedback gains or high amounts of noise, $u_2 \simeq -(u_1 + v_{y_1})$, which essentially cancels the first input and adds measurement noise into the command path. The frequency response estimates then degrade because the outputs exhibit lower signal-to-noise ratios. In these cases, the multisine amplitudes should be increased to excite the system, but should remain within flight test operational limits and regions of linearity.

D. Multiple Loop Closures

In this third simulation example, q was fed back to both δ_{eo} and δ_{ei}, with $C_{11} = C_{21} = -0.1$. The closed-loop short period mode had damping ratio 0.68 and frequency 7.7 rad/s (1.2 Hz), similar to the previous example.

Simulated measurements for this case are shown in Fig. 7. The control surface deflections had a pairwise correlation of 0.3, which was less than in the previous simulation example because the feedback gain was lower in value, even though both inputs contained feedback. The measured outputs had approximately the same magnitude as the previous case because roughly the same closed-loop dynamics were achieved. The inputs contained power at harmonic frequencies in both K_1 and K_2, due to the feedback.

To solve for the frequency responses, the output measurements were again expanded as in Eq. (8). In this case

$$\begin{aligned} u_1(\omega_2) &= A_1(\omega_2)\left[\mu_1(\omega_2) - C_{11}(\omega_2)y_1(\omega_2)\right] \\ &= -A_1(\omega_2)C_{11}(\omega_2)y_1(\omega_2) \end{aligned} \tag{20a}$$

$$\begin{aligned} u_2(\omega_1) &= A_2(\omega_1)\left[\mu_2(\omega_1) - C_{21}(\omega_1)y_1(\omega_1)\right] \\ &= -A_2(\omega_1)C_{21}(\omega_1)y_1(\omega_1) \end{aligned} \tag{20b}$$

which are both non-zero due to the feedback on all inputs. Solving for the frequency responses results in

$$H_{i1}(\omega_1) = \frac{y_i(\omega_1)}{u_1(\omega_1)} - \frac{H_{i2}(\omega_1)\,u_2(\omega_1)}{u_1(\omega_1)} \tag{21a}$$

$$H_{i2}(\omega_2) = \frac{y_i(\omega_2)}{u_2(\omega_2)} - \frac{H_{i1}(\omega_2)\,u_1(\omega_2)}{u_2(\omega_2)} \tag{21b}$$

Unlike the previous example, one frequency response can not be computed first and then substituted into the remaining equation; rather, more information must be obtained using interpolation and the entire set of unknown frequency responses solved simultaneously. In the limit as both control gains decrease, the basic approach is again recovered.

Expanding the system of linear equations for this case yields

$$\begin{bmatrix} \mathbf{b}_1 \\ \mathbf{b}_2 \\ \mathbf{0} \\ \mathbf{0} \end{bmatrix} = \begin{bmatrix} \mathbf{A}_{11} & \mathbf{0} \\ \mathbf{0} & \mathbf{A}_{22} \\ \mathbf{A}_{31} & \mathbf{A}_{32} \\ \mathbf{A}_{41} & \mathbf{A}_{42} \end{bmatrix} \begin{bmatrix} \mathbf{x}_1 \\ \mathbf{x}_2 \end{bmatrix} \tag{22}$$

The fourth partitioned row interpolates $H_{i1}(\omega_2)$ from $H_{i1}(\omega_1)$, similar to the third partitioned row. The interpolated equations make $\mathbf{A}$ a square matrix in this case without eliminating any variables or reducing the system.

The frequency response estimates computed using this method are shown in Fig. 8. Estimates using the general approach and output error matched the true frequency responses. Estimates using the basic approach were incorrect for both inputs, but were less inaccurate than for the previous example because the feedback gains were lower and used on both inputs.

The effect of frequency resolution on the interpolation was also investigated. For this example, as harmonic frequencies were discarded, frequency response estimates were accurate until all but five harmonic frequencies per input were discarded. For fewer harmonics, interpolation error was significant due to the relatively coarse frequency resolution.

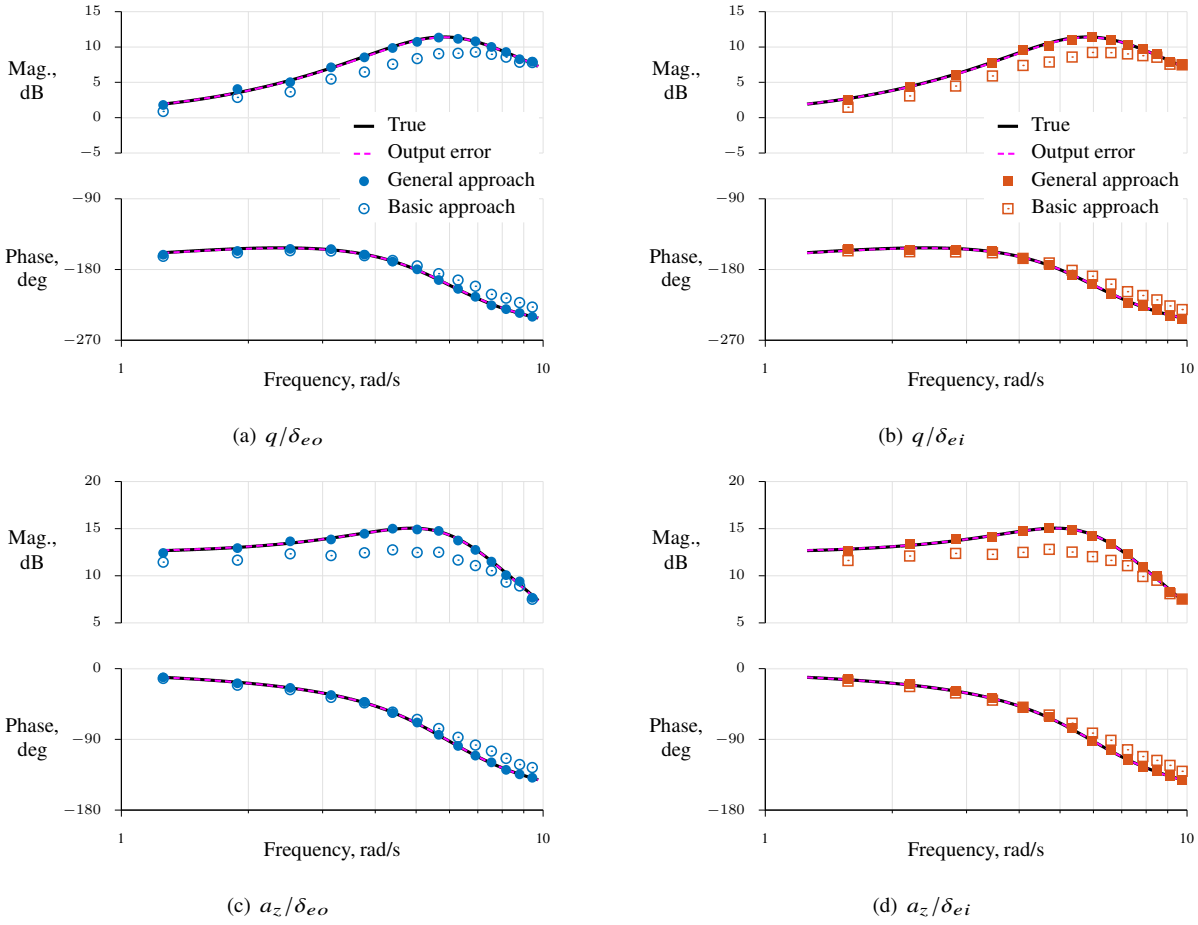

(a) q/δ_{eo} (b) q/δ_{ei}

(c) a_z/δ_{eo} (d) a_z/δ_{ei}

Fig. 8 Frequency response estimates for T-2 simulation with multiple loop closures.

E. Real-Time Estimation with Multiple Loop Closures

Although the preceeding cases were for batch estimation after all data were measured, this estimation can also be performed in real-time during the flight test. As input and output data are measured, recursive Fourier transforms are computed using Eq. (4). Then the system of linear equations in Eq. (22) is updated based on the new data, and estimates of the frequency responses evolve in time.

Although the matrix $\mathbf{A}$ can become large for many inputs, outputs, and frequencies, there are several aspects that reduce the computational burden for real-time computation. First, for a given experimental setup, the matrices $\mathbf{A}_{31}$, $\mathbf{A}_{32}$, $\mathbf{A}_{41}$, and $\mathbf{A}_{42}$ are computed and assembled once, before any data are collected, and remain fixed over time. As data are recorded, only $\mathbf{b}_1$, $\mathbf{b}_2$, $\mathbf{A}_{11}$, and $\mathbf{A}_{22}$ are updated from the measurements. Second, although Fourier transforms need to be computed at a sufficiently high rate, frequency responses can often be updated at a slower rate. For example, Fourier transforms describing rigid-body dynamics could be computed at 25 Hz, but then frequency responses can be computed and displayed at a slower rate such as 1 Hz. Last, the matrix $\mathbf{A}$ is sparse, so efficient routines for solving sparse systems can significantly reduce the amount of time needed to solve for the frequency responses when many inputs, outputs, and frequencies are considered.

An example real-time estimation is shown for the a_z/δ_{eo} frequency response in Fig. 9 using the data in the previous section where $C_{11} = C_{21} = -0.1$. Frequency responses are plotted for every data sample after the excitation began at 2.5 s. As more data are collected and the system attains steady-state oscillation, the frequency responses converge on the final estimates, which match the true curves and those estimated using output error. Errors in evaluating the Fourier transform with the Euler approximation and the chirp z-transform were negligible in this case. As discussed in Refs. [7, 15], some of the oscillations in the frequency response evolutions are due to evaluating the Fourier transforms at non-integer multiples of the harmonic frequencies. If desired, these errors and computation time can be reduced by only evaluating the estimates at times corresponding to integer numbers of cycles for each harmonic frequency. On average, about 0.1% of the sample period was needed to transform the data into the frequency domain, and 20% of the sample period was needed to solve for the frequency responses using a standard laptop computer running MATLAB®. The remaining 80% of the sample period could be used for refreshing displays, computing stability margins, or for processing additional outputs, inputs, and frequencies.

V. X-56A Flight Test Results

This section presents results using flight test data from the X-56A Multi-Use Technology Testbed (MUTT) airplane, which is shown in Fig. 10. The aircraft is a subscale aeroelastic demonstrator, designed for studying aeroelastic modeling and control technologies [16].

The maneuver analyzed was flown during Phase 1, Flight 11 and included multisines on five symmetric control surface pairs, applied after the aircraft was trimmed for straight and level flight at 48% fuel and 63% of the flutter speed.

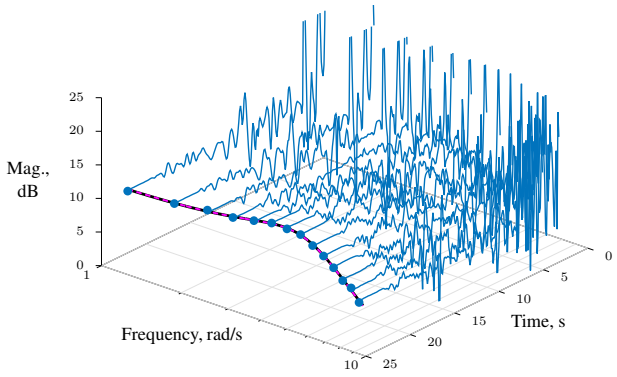

(a) a_z/δ_{eo} magnitude evolution.

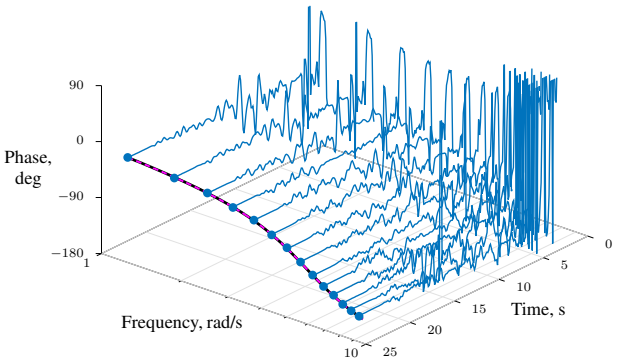

(b) a_z/δ_{eo} phase evolution.

Fig. 9 Real-time frequency response estimates for T-2 simulation with multiple loop closures.

Fig. 10 X-56A in flight (credit: NASA / Jim Ross).

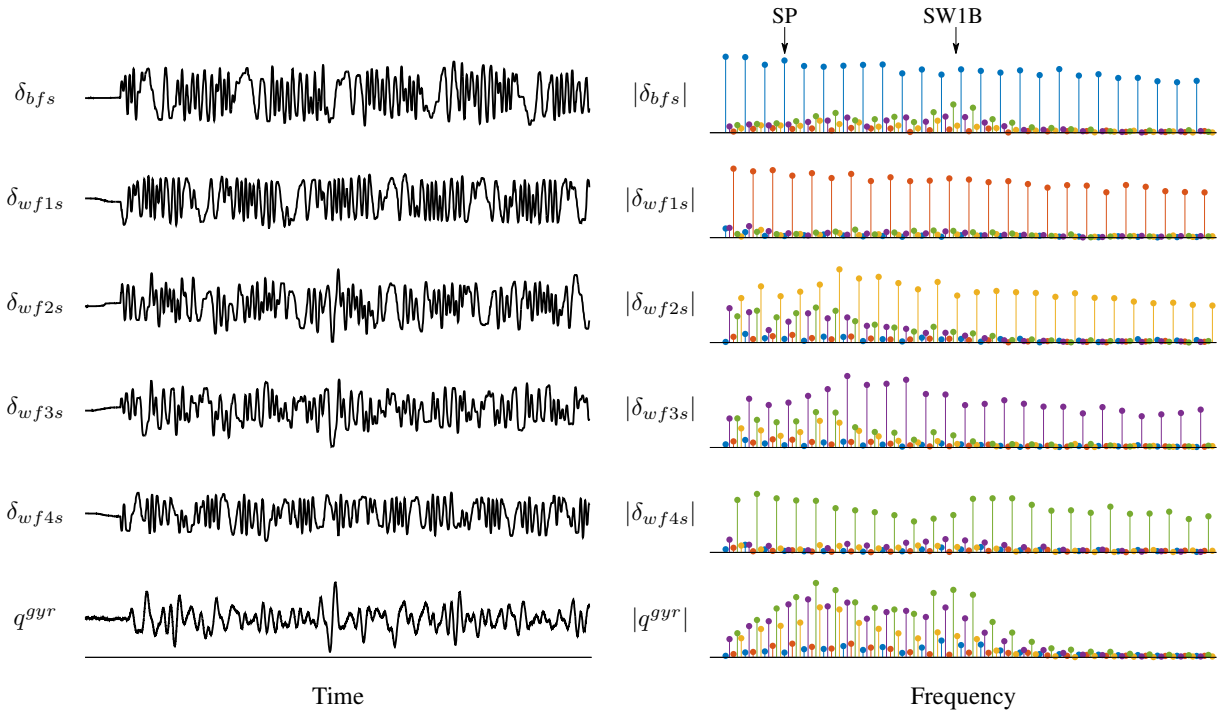

(a) Time histories.

(b) Fourier transform magnitudes.

Fig. 11 X-56A flight test data with feedback and mixing.

Measured pitch rate and combinations of measured vertical accelerations were fed back to the inner and outer control surface pairs δ_{bfs} and δ_{wf4s}. This feedback was also applied to the virtual elevator command, which was sent to the midspan surface pairs δ_{wf2s} and δ_{wf3s} equally. Therefore, both feedback and mixing were present during this maneuver. The effects of lateral-directional dynamics and pilot inputs were small for this maneuver.

The multisine perturbations, designated flight test aid (FTA) 503, were summed with other commands from the pilot and flight control system just before the actuator command position limiters. Time histories of the measured control surface deflections for one excitation period T are shown in Fig. 11(a). The inputs had correlations less than 0.24 in absolute value. Also shown is the output time history of a pitch-rate gyroscope, located near the nose of the aircraft. No numbers are given on the axes because the X-56A flight test data is ITAR restricted. However, these data represented small amplitude perturbations about the target flight condition.

The Fourier transform magnitudes for the input and output data are shown in Fig. 11(b). The multisines had 25 harmonics per input, uniform power, and a bandwidth spanning the short period (SP) and first symmetric wing bending mode (SW1B). Different colors are used to distinguish between the multisine design frequencies, as in the previous simulation examples. The plot is annotated with the identified SP and SW1B modal frequencies. The actuator dynamics created a mild roll-off in amplitude with frequency. The effects of feedback and mixing are evident in the additional frequency content of the signals, shown using multiple colors. The measured pitch rate contained content from all

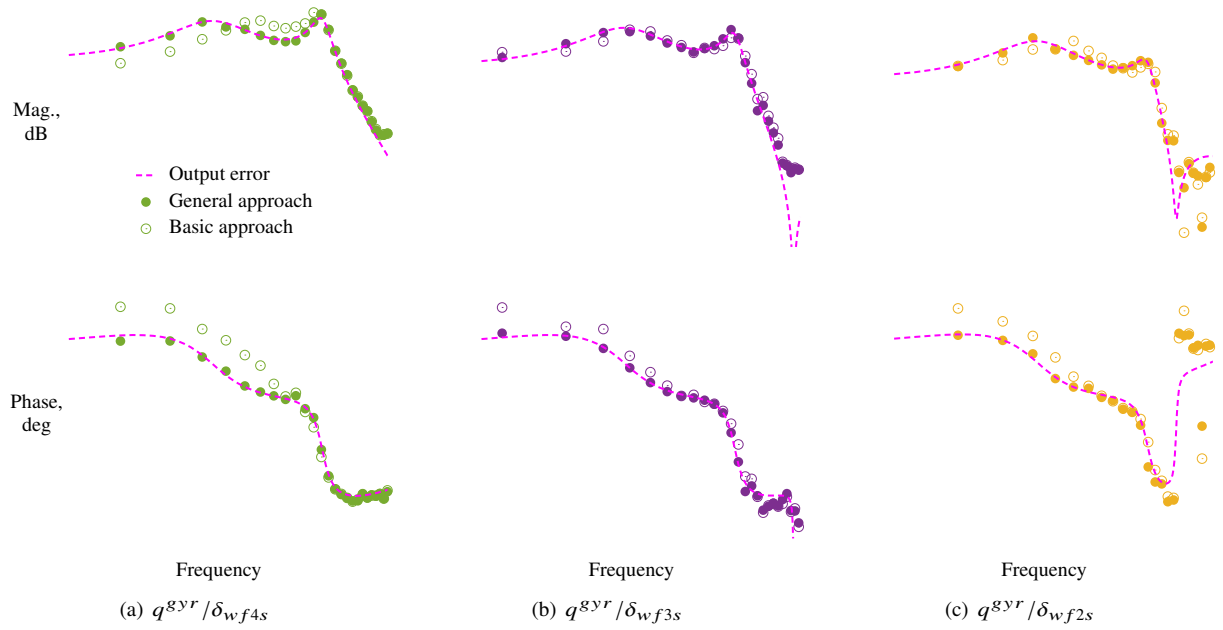

(a) q^{gyr}/δ_{wf4s} (b) q^{gyr}/δ_{wf3s} (c) q^{gyr}/δ_{wf2s}

Fig. 12 Frequency response estimates for X-56A flight test data with feedback and mixing.

harmonic frequencies, especially from the surface pairs δ_{wf2s}, δ_{wf3s}, and δ_{wf4s}.

Estimated frequency responses from the three outermost surfaces to the measured pitch rate are shown in Fig. 12. The same magnitude, phase, and frequency scales were used for each Bode plot. The amplitudes of the δ_{bfs} and δ_{wf1s} surfaces were too small to compute accurate frequency responses, as seen by the small magnitudes in the pitch-rate data in Fig. 11(b). The solid markers are estimates using the general approach, whereas the open markers are estimates using the basic approach. There are differences in the Bode plots for each frequency response, most prominently for q^{gyr}/δ_{wf4s}. These differences occur near the SP and SW1B modes, which is the bandwidth in which the control system operated. Results using the basic approach increased the SP frequency, lowered the SW1B frequency, and increased the phase angle. These characteristics are similar to the closed-loop results observed earlier for the T-2 simulation.

The dashed purple lines in Fig. 12 are the frequency responses for a state-space model identified using output error to match Fourier transforms of gyroscope and vertical accelerometer data in the frequency domain. In addition to estimating nondimensional stability and control derivatives for the aeroelastic model, time delays for each of the outputs were also estimated. More information about these results can be found in Ref. [17]. The frequency responses obtained using output error agreed with the frequency responses computed using the general method, similar to the previous T-2 simulation results.

VI. Conclusions

A method was developed for computing multiple-input multiple-output frequency response estimates of dynamic systems when the excitation inputs are orthogonal phase-optimized multisines injected at the actuator commands and feedback control or mixing is present. An earlier approach based on dividing Fourier transforms of measured output by input data at the frequencies in the multisine inputs was extended in this paper. The problem formulation began with an underdetermined system of linear equations. The system was made fully determined by including linear interpolations of the frequency responses between the multisine frequencies. The method was developed using example simulation data for the T-2 airplane in the open-loop and closed-loop configurations, using both post-flight and real-time computations. The method was also demonstrated using flight test data from the X-56A airplane flying under closed-loop control with control surface mixing.

The main findings of this research may be summarized as follows:

1) The method accurately estimates frequency responses when orthogonal phase-optimized multisines are used and when there is feedback or mixing present. Simulation and flight test results agreed with frequency responses obtained using an output-error analysis with frequency-domain data.
2) High multiple-input correlation was not detrimental for frequency response estimation using the general approach provided high signal-to-noise ratios were achieved. High multiple-input correlation was not detrimental for output-error parameter estimation provided all correlations were less than 0.9 in absolute value.
3) Linear interpolation was an adequate approach for obtaining additional information to solve for the unknown frequency response evaluations. Finer frequency resolution or higher-order interpolation should be used when there are lightly damped modes.
4) The basic approach for frequency response estimation was recovered in the limit as feedback and mixing decrease.
5) The method is suitable for real-time estimation during flight tests.

The method requires automated orthogonal, phase-optimized multisine inputs, good signal-to-noise ratios, and small pilot inputs to produce accurate results. Because frequency responses are used, steady-state and small-perturbation response data is needed. In addition, changes to the bare-airframe dynamics over the experiment duration, such as from fuel burn or variation in airspeed, must be small.

The method is procedural and does not require tuning parameters or engineering judgement to carry out the analysis. No specific knowledge of the control law or mixing scheme is needed. Feedback gains can be arbitrarily large so long as the multisines create responses with good signal-to-noise ratios. The general approach discussed extends the method from the previous basic approach, which is appropriate only for open-loop systems or single-input closed-loop systems. The real-time formulation can be used in applications such as real-time estimation, monitoring adaptive control laws during flight, sensor and actuator fault detection, real-time stability margin estimation during envelope expansion flights, and others.

Acknowledgments

This research was supported by the NASA Advanced Air Transport Technology (AATT) Project. T-2 flight data used in this work was generated by the NASA Langley (LaRC) AirSTAR team under the NASA Aviation Safety Program, Vehicle Systems Safety Technologies (VSST) project. Discussions with Eugene Morelli at LaRC on the approach are appreciated. The efforts of the X-56A team at NASA Armstrong Flight Research Center (AFRC) are gratefully acknowledged. Discussions with Christopher Miller, Jeffrey Ouellette, Jacob Schaefer, and the other X-56A team members about the flight test data and modeling results are appreciated.

References

[1] Morelli, E., and Klein, V., *Aircraft System Identification: Theory and Practice*, 2nd ed., Sunflyte, Williamsburg, VA, 2016.

[2] Klein, V., and Murphy, P., "Aerodynamic Parameters of High Performance Aircraft Estimated from Wind Tunnel and Flight Test Data," NATO Paper RTO-MP-11, 1998.

[3] Tischler, M., and Remple, R., *Aircraft and Rotorcraft System Identification: Engineering Methods with Flight Test Examples*, 2nd ed., AIAA, Reston, VA, 2012. doi:10.2514/4.868207.

[4] Ljung, L., *System Identification: Theory for the User*, 2nd ed., Prentice Hall, Upper Saddle River, NJ, 1999. doi:10.1109/MRA.2012.2192817.

[5] Knapp, M., Berger, T., Tischler, M., Cotting, M., and Marcus, A., "Development of a Full Flight Envelope F-16 VISTA Simulation Model from Closed-loop Flight Data," AIAA Paper 2018-0525, 2018. doi:10.2514/6.2018-0525.

[6] Berger, T., Tischler, M., Knapp, M., and Lopez, M., "Identification of Multi-Input Systems in the Presence of Highly Correlated Inputs," *Journal of Guidance, Control, and Dynamics*, Vol. 41, No. 10, 2018, pp. 2247–2257. doi:10.2514/1.G003530.

[7] Grauer, J., and Morelli, E., "Method for Real-Time Frequency Response and Uncertainty Estimation," *Journal of Guidance, Control, and Dynamics*, Vol. 37, No. 1, 2014, pp. 336–343. doi:10.2514/1.60795.

[8] Grauer, J., "Dynamic Modeling using Output-Error Parameter Estimation based on Frequency Responses Estimated with Multisine Inputs," NASA TM-2018-220108, November 2018.

[9] Morelli, E., "System IDentification Programs for AirCraft (SIDPAC)," version 4.1, NASA Software Catalog, `http://software.nasa.gov`, accessed December 2018.

[10] Morelli, E., "Multiple Input Design for Real-Time Parameter Estimation in the Frequency Domain," IFAC Paper REG-360, 2003. doi:10.1016/S1474-6670(17)34833-4.

[11] Morelli, E., "Flight-Test Experiment Design for Characterizing Stability and Control of Hypersonic Vehicles," *Journal of Guidance, Control, and Dynamics*, Vol. 32, No. 3, 2009, pp. 949–959. doi:10.2514/1.37092.

[12] Milliken, W., "Progress in Dynamic Stability and Control Research," *Journal of the Aeronautical Sciences*, Vol. 14, No. 9, 1947, pp. 493–519. doi:10.2514/8.1434.

[13] Pintelon, R., and Schoukens, J., *System Identification: A Frequency Domain Approach*, 2nd ed., John Wiley & Sons, Hoboken, NJ, 2012. doi:10.1002/9781118287422.

[14] Klein, V., "Aircraft Parameter Estimation in Frequency Domain," AIAA Paper 78-1344, 1978. doi:10.2514/6.1978-1344.

[15] Morelli, E., and Grauer, J., "Practical Aspects of the Frequency Domain Approach for Aircraft System Identification," AIAA Paper 2018-3477, 2018. doi:10.2514/6.2018-3477.

[16] Beranek, J., Nicolai, L., Buonanno, M., Atkinson, C., Holm-Hansen, B., and Flick, P., "Conceptual Design of a Multi-utility Aeroelastic Demonstrator," AIAA Paper 2010-9350, 2010. doi:10.2514/6.2010-9350.

[17] Grauer, J., and Boucher, M., "Identification of Aeroelastic Models for the X-56A Longitudinal Dynamics Using Multisine Inputs and Output Error in the Frequency Domain," *Aerospace*, Vol. 5, No. 2, 2019, pp. 1–25. doi:10.3390/aerospace6020024.